10

Finite Element Method Applied to the Modelling and Analysis of Induction Motors

M'hemed Rachek and Tarik Merzouki
University Mouloud Mammeri of Tizi-Ouzou
Algeria

1. Introduction

During the past decades, the development of solution methods and the growth of computer capacities have made its possible to solve more and more involved magnetic field problems. Thus, numerical techniques essentially based on the Finite Elements Method (FEM) have been used and has gradually become a standard in electrical machine modelling-design, analysis and optimisation. Electrical machines are electromagnetic devices with combined constrains such as complex geometries and several physical phenomena's. To model them, we must solve the magnetic field non-linear Partial Differential Equation (PDE) derived from the Maxwell's equations combined to the materials properties, and their coupling with phenomena that exist in electromagnetic structures, such as electric circuits, and mechanical motional equations. (Arkkio, 1987; Benali, 1997).

Induction Motor (IM) is an electromagnetic-mechanical actuator where strongly interacts several phenomena such as magnetic field, electrical circuits, mechanical motion. The aim of this chapter is to present an implementation of the finite element method for the modelling of rotating electrical machines, especially the squirrel cage three-phase induction motors. The generalized model consists firstly on strong coupling between the partial differential equation of the magnetic field diffusion and the electric circuits equations obtained from Kirchhoff laws. The model integrates as well realistic geometries, and the non-linear properties of the magnetic materials, as voltage supply of the stator windings. Secondly, the mechanical equation including the rotor movement effects is coupled to the electromagnetic phenomenon through the magnetic force responsible of the rotor motion.

The governing magnetic field time-dependent equation derived from Maxwell formalism is expressed in term of Magnetic Vector Potential (MVP) with only z-direction component for the cases of two dimensional (x,y) cartesian coordinates. The induction motors stator windings are usually in star or delta connection, then the source term of the magnetic field is explicitly an applied line voltage or implicitly the magnetizing current. The squirrel rotor cage is formed by massive conductive bars short-circuited at their ends through massive and conductive end-rings. Mathematically, the squirrel rotor cage appear as a polyphases circuits modelled by the same way that the stator windings but with affecting a zero voltage for each adjacent bars with theirs end-rings portion.

Generally, permittivity and conductivity can be considered as constants, however the magnetic reluctivity of the core ferromagnetic materials depend on the magnetic flux density intensity which is implicitly fixed by the voltage excitation or currents level at each step time of the motor operating. This magnetic flux density-reluctivity non linear dependence is take into account in the model by the classical iterative Newton-Raphson method. The finite element formulation of the non-linear transient coupled magnetic field-electric circuits of induction motors model leads to an algebraic differential equations system. The solution process requires firstly a major loop concerning the time-discretization using the effectiveness Cranck-Nicholson scheme, and secondly for each step time we have to unsure the minor loop convergence of the Newton-Raphson algorithm for determining the appropriate magnetic reluctivity values.

The time stepping finite magnetic field-electric circuits coupled model is sequentially coupled with the mechanical equation of the rotor motion. The interaction between stator and rotor flux densities generate an electromagnetic torque responsible of the motion. Since the physical position of the moving part of the induction motors will change at each time step, the finite element coefficients matrix are consequently changes. The unknown mechanical position of the moving part can be found after solving the mechanical motional equation by the fourth order Rung-Kutta method. To take the movement into account, several strategies have been proposed, the boundary integral method, the air-gap-element, and the connecting meshes through the sliding line, moving band, and the Lagrange multipliers or nodal interpolation techniques (Dreher, et al., 1996).

A particularly elegant and accurate method is that due to (Abdel-Razek, et al., 1982) named the Air-Gap Element (AGE). The air gap element consist on the coupling between the meshes of the stator and rotor through the unmeshed air-gap band. The air-gap appears such as a multi-nodes finite element (Macro-Element) where it corresponding Laplace equation solution leads to an analytical expression of the magnetic vector potential. The combination between the magnetic vector potential of the air gap interfaces leads to a macro-element matrix. At each displacement step the rotor movement is simulated through only new computation of the air-gap element matrix, then the rotor implicitly moved without any changes on the motor mesh topologies. In addition, since the magnetic vector potential is derived from the field analytical solution in the air-gap, the magnetic flux density can be directly deduced permitting an accurate calculation of the electromagnetic torque using the Maxwell stress tensor method.

The magnetic-electric model obtained from the strong coupling of electric circuit equations of stator windings and polyphases rotor squirrel cage and the magnetic vector potential diffusion equations of the magnetic field, are solved using the nodal based finite element method with step-by-step algorithm. Finally, the magnetic vector potential, stator windings currents and bars voltages differences are the unknown variables. The studied simulation concerns different operating modes such as electrical transients where the speed is constant for no-load and nominal conditions, and the general no-load and loaded electro-magneto-mechanical transient mode. Despite complex mathematical background, the simply and detailed presentation of the model offers an important aid for students, teachers and industrial employers for understanding the basis in simulation of electrical machines and particularly induction motors.

2. Magnetic field native equations

The theory of electromagnetic electrical machines modeling is described by the time-space differential Maxwell's equations where the displacement current are neglected because of the low frequency oft he supply source (Joao, et al., 2003; Binns, et al.,1994; Arkkio, 1987):

$$\nabla \times H = J \tag{1}$$

$$\nabla \times E = -\frac{\partial B}{\partial t} \tag{2}$$

$$\nabla \cdot B = 0 \tag{3}$$

Moreover the electric and magnetic fields quantities are related with the material properties expressed by the following constitutive relations:

$$H = \upsilon\left(B^2\right) \cdot B \tag{4.a}$$

$$J = \sigma \cdot E \tag{4.b}$$

Where $\upsilon\left(B^2\right)$ ist he magnetic reluctivity, σ the electric conductivity, H is the magnetic field, and J the conduction current density.

In the frequency domain and time-dependence with taking into account the eddy current, through (2) and (3) the electric field E and the magnetic flux density B are expressed using the magnetic vector potential A and scalar electric potential U^r, such as :

$$E = -\frac{\partial A}{\partial t} + \nabla U^r \tag{5}$$

$$B = \nabla \times A \tag{6}$$

Two types of conductors are considered in the field model parts. A solid conductor corresponds to a massive part of conductive material in the computational domain, whereas a stranded conductor models and thereby assumes the current to be homogeneously distributed along the cross-section of the coil. The positive or negative direction of the current is fixed by the unit vector $d = \pm 1$, as follow.

$$J = \begin{cases} d\dfrac{N_{cn} I_n^s}{S_n} & \text{Stranded stator conductors} \\ -\sigma\dfrac{\partial A}{\partial t} + \sigma\left(\nabla U_m^r\right) & \text{Solid conductors rotor bars} \end{cases} \tag{7}$$

To formulate the magnetic field problem, we consider a two-dimensional domain partitioned into electrically conducting and non-conducting regions as shown in Fig.1. This domain represents for instance the cross-section of an induction motor with length L_δ. The conducting regions are the cross-sections of stranded stator windings conductors Ω_s and

solid conductors Ω_b of the rotor bars, the non-conducting ferromagnetic region Ω_{core}, and the air gap region by Ω_{air}.

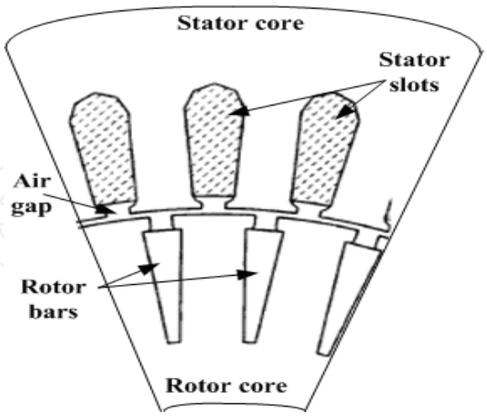

Fig. 1. Geometrical configuration of induction motors

To develop the mathematical model in term of magnetic vector potential in the three-phase induction motor, it is assumed that the magnetic field lies in the cross-sectional two-dimensional (x, y) plane. Hence, only the z-component of the induced current and the magnetic vector potential can be considered. It also assumes that magnetic material of the motor cores is non-linearly isotropic. The magnetic property of the laminated iron cores is modelled by Marrocco approximation of the recluctivity (Brauer, et al, 1985; Hecht, et al., 1990), which is a single-valued nonlinear function of the flux density B, thus exclude the effect of magnetic hysteresis from the analysis.

The fundamental equations obtained from (1)-(6) and describing the time-space variation of the magnetic vector potential with the component $A = (0, 0, A_z(x, y, t))$ has the following form

$$\frac{\partial}{\partial x}\left(\upsilon(B^2)\frac{\partial A_z(x,y,t)}{\partial x}\right)+\frac{\partial}{\partial y}\left(\upsilon(B^2)\frac{\partial A_z(x,y,t)}{\partial y}\right)= -d\frac{N_{cn}I_n^s}{S_n}+\sigma\left(-\frac{\partial A_z(x,y,t)}{\partial t}+\frac{U_m^r}{L_\delta}\right) \quad (8)$$

In the model of an electrical machine, the magnetic field due to the currents in the coils. However, it is often more appropriate to model the feeding circuit as a voltage source, which leads to the combined solution of the magnetic field and circuit equations. The stator phase windings are generally modelled as filamentary conductors, and the rotor bars are modelled as solid conductors with eddy currents.

3. Electric circuits equations model

The computational model of the induction motors can be greatly improved by coupling the circuit equations of the stator and rotor windings with the two-dimensional field equation (8). In the circuit equations, the dependence between current and voltage is solved and the circuit quantities are coupled with the magnetic field by means of flux linkage. Also, the end-windings outside the core region are modelled by including an additional inductance in the circuit model (Hecht, et al., 1990; Kanerva, 2005; Piriou, et al., 1990).

3.1 Electric circuits equations of the stator windings

The delta and star connection (see Fig. 2 and Fig.3) are the two commonly used ways to connect the stator windings. In the delta connection the potential differences induced in the stator windings are equal to the line voltages. In the star connection with neutral point, the potential differences of the stator windings are equal to the phase voltages.

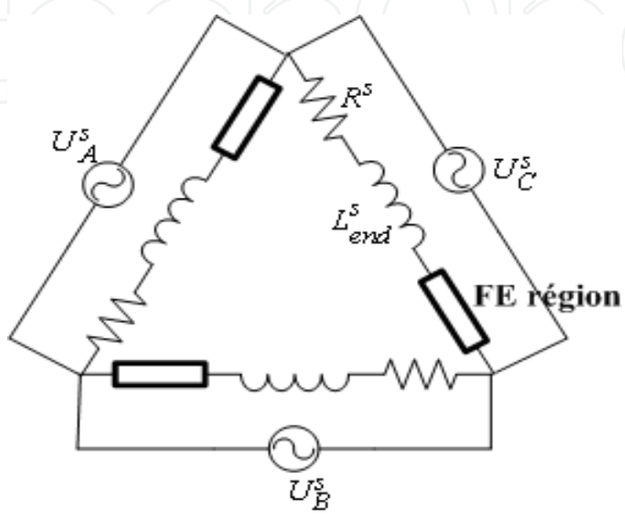

Fig. 2. Stator windings in delta connection.

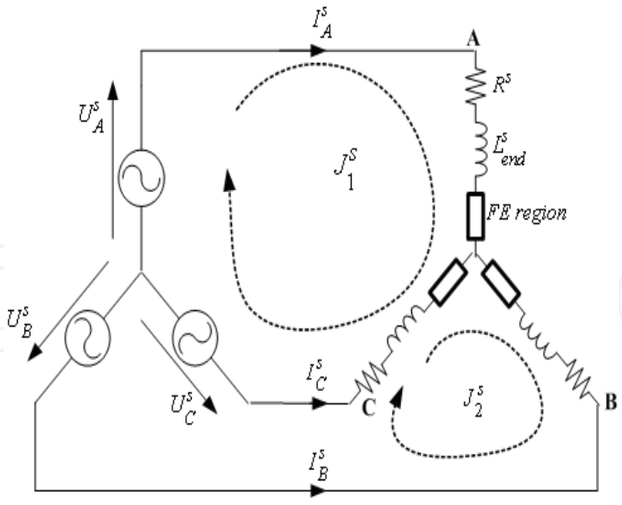

Fig. 3. Stator windings in star connection.

The three phases stator circuit equations are in matrix form:

$$U^s(t) = E^s(t) + R^s I^s(t) + L^s_{end} \frac{dI^s(t)}{dt} \tag{9}$$

$$E_n^s(t) = N_s\left(\frac{L_\delta N_{cn}}{S_n}\right)\sum_{n=1}^{N_{cn}}\left(\iint_{\Omega_{s_n}^+}\left(\frac{\partial A}{\partial t}\right)d\Omega - \iint_{\Omega_{s_n}^-}\left(\frac{\partial A}{\partial t}\right)d\Omega\right) \qquad n = A,B,C \tag{10}$$

Where A,B,C denote the three stator phase, Ω_s^+ and Ω_s^- are respectively, the cross-sectional areas of the "go" and "return" side of the phase conductors. The column vectors of the potential differences of the stator windings with their currents and electromotive force are detailed as follows:

$$U^s(t) = \begin{Bmatrix} U_A^s(t) \\ U_B^s(t) \\ U_C^s(t) \end{Bmatrix} \quad , \; E^s(t) = \begin{Bmatrix} E_A^s(t) \\ E_B^s(t) \\ E_C^s(t) \end{Bmatrix} \quad , \; I^s(t) = \begin{Bmatrix} I_A^s(t) \\ I_B^s(t) \\ I_C^s(t) \end{Bmatrix} ,$$

$$R^s = \begin{pmatrix} R_A^s & 0 & 0 \\ 0 & R_B^s & 0 \\ 0 & 0 & R_C^s \end{pmatrix} , \; L_{end}^s = \begin{pmatrix} L_{end_A}^s & 0 & 0 \\ 0 & L_{end_B}^s & 0 \\ 0 & 0 & L_{end_C}^s \end{pmatrix}$$

When the stator windings has star connection with non-connected neutral star point (see Fig. 3), only two from the three phase currents are independent variables, and the third is determined by an additional constraint which unsure a zero sequence of the phases currents $I_C^s = -I_A^s - I_B^s$. For this reason the connectivity matrix is formed:

$$[K] = \begin{bmatrix} 1 & 0 & -1 \\ 0 & 1 & -1 \end{bmatrix} \tag{11}$$

The line voltages V^s and loops currents $J_{1,2}^s$ containing the two independent currents, are formed in the following way:

$$K\begin{Bmatrix} U_{AN}^s \\ U_{BN}^s \\ U_{CN}^s \end{Bmatrix} = \begin{bmatrix} 1 & 1 & 0 \\ 0 & 1 & 0 \end{bmatrix}\begin{Bmatrix} U_{AB}^s \\ U_{BC}^s \\ U_{CA}^s \end{Bmatrix} = Q^s\left\{V^s\right\} \tag{12.a}$$

$$\left\{I^s\right\} = [K]^{tr}\begin{Bmatrix} J_1^s \\ J_2^s \end{Bmatrix} = [K]^{tr}\begin{Bmatrix} I_A^s \\ I_B^s \end{Bmatrix} = [K]^{tr}\left\{J_{1,2}^s\right\} \tag{12.b}$$

3.2 Electric circuits equations of the rotor cage

A network of the non-skewed rotor cage is shown in Fig. 4. For normal operating frequencies (50 or 60 Hz), the inductive component of the inter-bar impedance can be neglected. Two adjacent bars are connected by the end-ring resistances and inductances (Arkkio, 1987; Benali, 1997; Ho, et al., 2000).

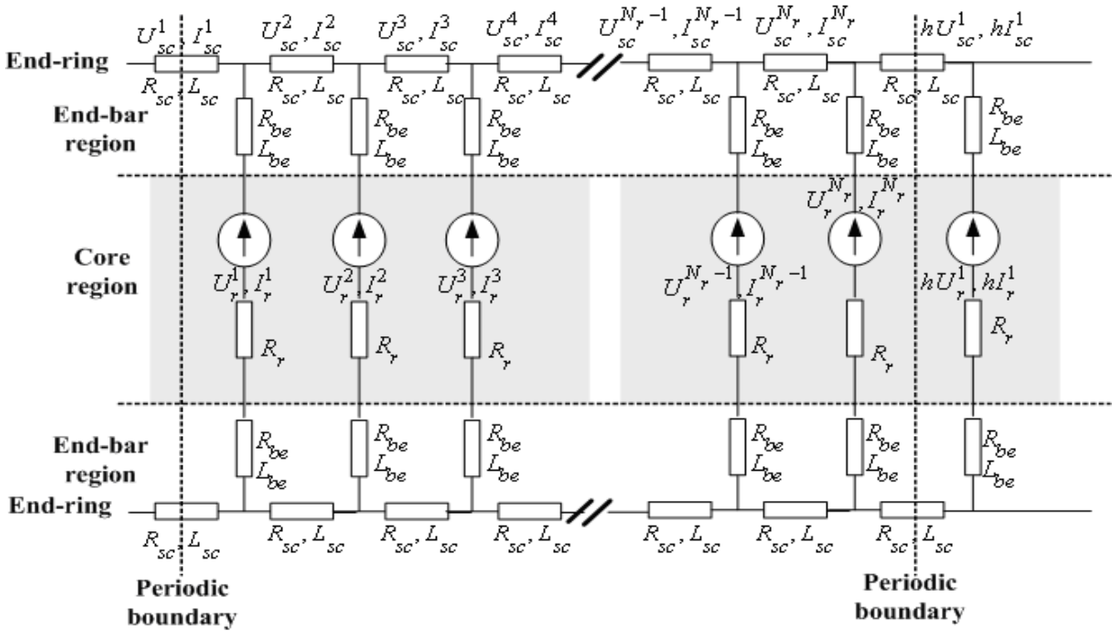

Fig. 4. Electric circuit configuration of squirrel rotor cage.

In a cage rotor, each rotor bar requires its own equation. In time variation, the potential difference induced in the m^{th} rotor bar is given by:

$$U_m^b = R_r I_m^r + R_r \iint_{\Omega} \beta_m^r \sum_{j=1}^{N_d} \left(N_j \frac{\partial A_j}{\partial t} \right) d\Omega \qquad m = 1,...,N_b \tag{13}$$

$$\beta_m^r = \begin{cases} 1 & \text{if } (x,y) \text{ belongs to rotor bar } m \\ 0 & \text{Otherwise} \end{cases} \tag{14}$$

Where R_r is $(N_b \times N_b)$ unit matrix.

Integration of the current density in a rotor bar over its cross section S_b gives the total currents of the m^{th} bar. When constant conductivity and uniform cross section area S_b are assumed in the bar and the end-bar, $(N_b \times N_b)$ unit end-bars self inductance L_{be}, and resistance R_{be} matrices are included, the above equation (13) for each bar can be expressed by (15) and (17). All the rotor bars are connected by short-circuit rings in both ends of the rotor core (16). This is taken into account by defining the end-ring unit resistance matrix and the end-ring unit inductance matrix.

$$U_m^r = R_{be} I_m^b + L_{be} \frac{dI_m^b}{dt} + U_m^b \tag{15}$$

$$U_m^{sc} = R_{sc} I_m^{sc} + L_{sc} \frac{dI_m^{sc}}{dt} \tag{16}$$

$$I_m^r = \sigma\left(\iint_{\Omega_b}\left(-\frac{\partial A}{\partial t}+\frac{U_m^r}{L_\delta}\right)d\Omega\right) \tag{17}$$

From Kirchhoff's second law applied to the rotor cage electric circuit (Fig.4), a relation between the potential difference and currents of bars and end-ring are obtained such as:

$$2U^{sc} = M\cdot U^b \tag{18.a}$$

$$I^b = M^{tr}\cdot I^{sc} \tag{18.b}$$

Where M ist he rotor cage connection matrix, and h is the periodicity factor h (+1 if periodic and -1 if non-periodic).

$$M=\begin{bmatrix}1&0&.&.&.\\0&1&.&.&.\\.&.&.&.&.\\.&.&.&.&0\\.&.&.&0&1\end{bmatrix}+\begin{bmatrix}0&0&.&.&.\\-1&0&.&.&.\\.&-1&.&.&.\\.&.&.&.&0\\.&.&.&-1&0\end{bmatrix}+\begin{bmatrix}0&0&.&.&-h.\\0&0&.&.&.\\.&.&.&.&.\\.&.&.&.&0\\.&.&.&0&0\end{bmatrix} \tag{19}$$

4. Magnetic field – Electric circuits coupling

4.1 Time stepping finite element formulation of the non-linear magnetic field model

In the electric machine model, the magnetic field in the iron core, windings and air gap is solved by the two-dimensional finite element code and coupled with the voltage equations of the stator and rotor windings. The model is based on the direct coupling, which means that magnetic field equations and electrical circuit equations are solved simultaneously by time-stepping approach with handling magnetic non-linearities using Newton-Raphson iterative algorithm.

In the time stepping formulation, the derivative of the vector potential, stator windings currents and bars voltages are approximated by first-order difference ratios:

$$\frac{\partial}{\partial t}\begin{Bmatrix}A\\I_n^s\\U_m^s\end{Bmatrix}=\frac{1}{\Delta t}\begin{pmatrix}A\\I_n^s\\U_m^r\end{pmatrix}_{k+1}-\begin{pmatrix}A\\I_n^s\\U_m^r\end{pmatrix}_{k}\Bigg) \tag{20}$$

The time discretization is performed by using the Crank-Nicholson sheme as:

$$\begin{Bmatrix}A\\I_n^s\\U_m^r\end{Bmatrix}_{k+1}=\frac{1}{2}\left\{\begin{pmatrix}\frac{\partial A}{\partial t}\\\frac{\partial I_n^s}{\partial t}\\\frac{\partial U_m^r}{\partial t}\end{pmatrix}_{k+1}+\begin{pmatrix}\frac{\partial A}{\partial t}\\\frac{\partial I_n^s}{\partial t}\\\frac{\partial U_m^r}{\partial t}\end{pmatrix}_{k}\right\}\Delta t+\begin{Bmatrix}A\\I_n^s\\U_m^r\end{Bmatrix}_{k} \tag{21}$$

Several methods can be used for the numerical solution of the magnetic field equation (8), such as reluctance networks, the boundary element method, the finite difference method or the finite element method. In this work, the numerical analysis is based on the finite element method. The two-dimensional geometry is covered by a finite element mesh, consisting of first-order triangular elements. If possible, the cross section of the electrical machine is divided in N_s symmetry sectors, from which only one is modelled by the finite element method and symmetry constraints are set on the periodic or anti-periodic boundary (Nougier, 1999; Binns, et al., 1994; Ho, et al., 1997). The magnetic vector potential can be approximated as the sum of the element shape functions times and nodal potential values:

$$A_z(x,y,t) = \sum_{j=1}^{N_{nodes}} N_j(x,y) \cdot A_{zj}(x,y,t) \tag{22}$$

Where N_{nodes} is the total nodes number of the finite element mesh, $N_j(x,y)$ the shape function, and $A_{zj}(x,y,t)$ is the magnetic vector potential of the node j .

The numerical field equation is derived by Galerkin's method, where (8) is multiplied by shape functions and integrated over the whole finite element mesh with substituting the magnetic vector potential approximation (22). The last line integral term of the formulation (23) correspond to the air-gap contribution due to the rotor movement.

$$\iint_{\Omega} \sum_{j=1}^{N_{nodes}} \left[\upsilon\left(B^2\right)\left(\nabla N_i\right)\cdot\left(\nabla N_j\right)\left\{A_j\right\} + \left(\sigma N_i N_j \frac{\partial\left\{A_j\right\}}{\partial t} \right) \right] d\Omega +$$

$$\iint_{\Omega} \left\{ \sum_{j=1}^{N_{nodes}} \left(-\sigma N_i \left(\beta_m^s U_m^r \right) - N_i \left(\beta_n^s I_n^s \right) \right) \right\} d\Omega = \tag{23}$$

$$\oint_{\Gamma} \upsilon_o \left(\frac{\partial \sum_{j=1}^{nnt} N_j^{AGE} A_j^{AGE}}{\partial n} \right) d\Gamma$$

The problems in the analysis of the electrical machine are almost non-linearly isotropic due to the presence of ferromagnetic materials. The magnetic permeability is non-homogeneous and will be a function of the local magnetic field which is unknown at the start of the problem. The permeability is low at very low flux densities, rises quickly as the flux density increases and then decreases in the saturation region. As the permeability is unavoidably contained in all of the element stiffness matrices, an iterative process must be used to keep correcting the permeability until it consistent with the field solution. The Newton-Raphson iterative technique is used for the analysis of the non-linear problem (Brauer, et al., 1985; Joao, et al.,2003; Neagoe, et al., 1994).

At the beginning, an unsaturated value of permeability is assigned for each element of the mesh. When solving the problem, the magnitude of the flux density in each element is computed and the magnetic reluctivities are corrected to be consistent with the computed

values of the flux density. The problem is then solved again using the new values. This process is continued till a satisfactory result is obtained when the difference between the actual solution and the previous one is smaller than a pre-specified value. The equations for the time-stepping simulation are derived by adding the equations from two successive steps together and replacing the derivatives with expressions (20) and (21). Using this approach, the magnetic vector potential integrals formulation (23) are formed for each node in the finite element mesh. Following, a residual vector $\Re^f$ is obtained after the finite element discretization, and the i^{th} element of the residual vector is:

$$\begin{aligned}\Re_i^f\left(A_{k+1},U_{n_{k+1}}^r,I_{nk+1}^s\right)= &\iint_\Omega\left\{\sum_{j=1}^{N_n}\left(\nu(A_{k+1})(\nabla N_i)\left(\nabla N_j\right)+\frac{2\sigma}{\Delta t}N_iN_j\right)A_j\Big|_{k+1}\right\}d\Omega\\ -\iint_\Omega&\left\{N_i\frac{\sigma}{L_\delta}\sum_{m=1}^{N_b}\beta_m^r\left(U_m^r\Big|_{k+1}\right)+N_i\sum_{n=A,B,C}\beta_j^s\left(I_n^s\Big|_{k+1}\right)\right\}d\Omega\\ +\iint_\Omega&\left\{\sum_{j=1}^{N_n}\left(\nu(A_k)(\nabla N_i)\left(\nabla N_j\right)-\frac{2\sigma}{\Delta t}N_iN_j\right)A_j\Big|_{k+1}\right\}d\Omega\\ -\iint_\Omega&\left\{N_i\frac{\sigma}{L_\delta}\sum_{m=1}^{N_b}\beta_m^r\left(U_m^r\Big|_k\right)+N_i\sum_{n=A,B,C}\beta_n^s\left(I_n^s\Big|_k\right)\right\}d\Omega-\oint_\Gamma\upsilon_o\frac{\partial}{\partial n}\left(\sum_{j=1}^{nnt}N_j^{AGE}\cdot A_j^{AGE}\right)d\Gamma\end{aligned} \tag{24}$$

In matrix form, equation (24) can be written as follows:

$$\begin{aligned}\Re_i^s\left(A_{k+1},U_{nk+1}^r,I_{nk+1}^s\right)= &\left[S\left(A_{k+1}\right)+M\left(A_{k+1}\right)+S^{AGE}\left(A_{k+1}\right)\right]\left\{A_{k+1}\right\}+\left(D^r\right)^TU_{k+1}^r\\ +\left(D^{sT}K^T\right)&\left(J_{1,2}^s\right)_{k+1}+\left[S\left(A_k\right)+M\left(A_k\right)+S^{AGE}\left(A_k\right)\right]\left\{A_k\right\}+\left(D^r\right)U_k^r+\left(D^{sT}K^T\right)\left(J_{1,2}^s\right)_k\end{aligned} \tag{25}$$

4.2 Time stepping finite element formulation of the stator windings equations

The same approximation (20), and (22) is also applied to the winding equations (9) and (10). The resulting equations of the average value of the potential difference at the time steps *k* and *k+1* is used to approximate the true potential difference as:

$$U_n^s\Big|_{k+1}=\left(R^sI_n^k+L_{end}^s\frac{dI_n^s}{dt}\right)\Big|_{k+1}+N_sL_z\int_\Omega\beta_n^s\frac{\partial A}{\partial t}\Big|_{k+1}d\Omega \tag{26.a}$$

$$U_n^s\Big|_k=\left(R^sI_n^s+L_{end}^s\frac{dI_n^s}{dt}\right)\Big|_k+N_sL_z\int_\Omega\beta_n^s\frac{\partial A}{\partial t}\Big|_k d\Omega \tag{26.b}$$

$$\beta_n^s=\frac{N_{cn}}{S_n}\begin{cases}-1 & \text{Negatively oriented coil}\\ +1 & \text{Positively orriented coil}\\ 0 & \text{Otherwise}\end{cases} \tag{27}$$

After the substitution of the approximation (21) in (26), the voltages equations of the n^{th} phase of the stator windings becomes:

$$\frac{U_n^s\big|_{k+1}+U_n^s\big|_k}{2}=N_sL_z\iint_{\Omega}\beta_n^s\sum_{j=1}^{N_d}N_j\left(\frac{A_j\big|_{k+1}+A_j\big|_k}{\Delta t}\right)d\Omega+\frac{R^s}{2}\left(I_n^s\big|_{k+1}+I_n^s\big|_k\right)+L_{end}^s\frac{I_n^s\big|_{k+1}+I_n^s\big|_k}{\Delta t} \quad (28)$$

The voltages equations (28) are expressed in matrix form as follow:

$$\begin{aligned}\Re_i^s\left(A_{k+1},I_{nk+1}^s\right)= &\left(KD^s\right)A_{k+1}+\left(-\frac{R^s\Delta t+2L_{end}^s}{2N_sL_\delta}\right)KK^T\left(J_{1,2}^s\right)_{k+1}-\\ &\left(KD^s\right)A_k+\left(-\frac{R^s\Delta t-2L_{end}^s}{2N_sL_\delta}\right)KK^T\left(J_{1,2}^s\right)_k+\left(\frac{\Delta t}{2N_sL_\delta}\right)Q^s\left[\left(V_n^s\right)_{k+1}+\left(V_n^s\right)_k\right]\end{aligned} \quad (29)$$

Equation (29) can be written under this following form:

$$\begin{aligned}\Re_i^s\left(A_{k+1},I_{nk+1}^s\right)=&\left(KD^s\right)A_{k+1}+\left(G^sKK^T\right)\left(J_n^s\right)_{k+1}-\left(KD^s\right)A_k\\ &+\left(H^sKK^T\right)\left(J_{1,2}^s\right)_k+\left(C^s\right)\left[\left(V_n^s\right)_{k+1}+\left(V_n^s\right)_k\right]\end{aligned} \quad (30)$$

The different matrix components of (30) are:

$$D_{ij}^s=-\iint_{\Omega^e}\left(\beta_n^s\cdot N_j\right)d\Omega^e \quad (31.a)$$

$$\left[G^s\right]_{(3\times3)}=-\left(\frac{R^s\Delta t+2L_{end}^s}{2N_sL_\delta}\right) \quad (31.b)$$

$$\left[H^s\right]_{(3\times3)}=-\left(\frac{R^s\Delta t-2L_{end}^s}{2N_sL_\delta}\right) \quad (31.c)$$

$$\left[C^s\right]_{(3\times3)}=\left(\frac{\Delta t}{2N_sL_\delta}\right)Q^s \quad (31.d)$$

4.3 Time stepping finite element formulation of the rotor cage equations

By undertaking the same way as the stator windings, after applying Crank-Nicholson scheme, equations (13), (16) and (17) of the voltage equations of the rotor cage becomes:

$$\frac{1}{2}\left(U_m^b\big|_{k+1}+U_m^b\big|_k\right)=\frac{1}{2}R_r\left(I_m^r\big|_{k+1}+I_m^r\big|_k\right)+R_r\int_{\Omega}\beta_m^r\sigma\left\{\sum_{j=1}^{N_d}\frac{A_j\big|_{k+1}-A_j\big|_k}{\Delta t}\right\}d\Omega \quad (32)$$

$$\frac{1}{2}\left(U_m^r\Big|_{k+1}+U_m^r\Big|_k\right)=\frac{R_r}{2}\left(I_m^r\Big|_{k+1}+I_m^r\Big|_k\right)+\ L_{be}\frac{\left(I_m^r\Big|_{k+1}+I_m^r\Big|_k\right)}{\Delta t}+\frac{1}{2}\left(U_m^b\Big|_{k+1}+U_m^b\Big|_k\right) \tag{33.a}$$

$$\frac{1}{2}\left(U_m^{sc}\Big|_{k+1}+U_m^{sc}\Big|_k\right)=\ \left(\frac{R_{sc}}{2}+\frac{L_{sc}}{\Delta t}\right)\left(I_m^{sc}\Big|_{k+1}+I_m^{sc}\Big|_k\right) \tag{33.b}$$

The combination of the expressions (32) and (33) with the end-rings voltages and currents (18), lead to the matrix form of the unified loops voltages equations in the rotor cage expressed as:

$$\Re\left(A_{k+1},U_{mk+1}^r\right)=\ \left(D^r\right)A_{k+1}+\left(C^r\right)\left(U_m^r\right)_{k+1}+\ \left(-D^r\right)A_k+\left(C^r\right)\left(U_m^r\right)_k+\left(G^r\right)\left(I_m^r\right)_k \tag{34}$$

$$\left[C^r\right]_{(N_b\times N_b)}=\frac{\Delta t}{2L_\delta R_b}\times\left\{I_{N_b\times N_b}+\frac{R_b}{2}\left[\left(R_{sc}+2\frac{L_{sc}}{\Delta t}\right)I_{(N_b\times N_b)}+\left(R_{be}+2\frac{L_{be}}{\Delta t}\right)M_b\right]^{-1}M_b\right\} \tag{35.a}$$

$$\begin{aligned}G^r=\frac{\Delta t}{2L_\delta}I_{N_b\times N_b}-\ \ &\frac{\Delta t}{2L_\delta}\left[\left(R_{sc}+2\frac{L_{sc}}{\Delta t}\right)I+\left(R_{be}+2\frac{L_{be}}{\Delta t}\right)M_b\right]^{-1}\\ &\times\ \left[\left(R_{sc}-2\frac{L_{sc}}{\Delta t}\right)I+\left(R_{be}-2\frac{L_{be}}{\Delta t}\right)M_b\right]\end{aligned} \tag{35.b}$$

$$D_{ij}^r=-\frac{\sigma}{L_\delta}\int_\Omega\left(\beta_i^r\cdot N_j\right)d\Omega \tag{35.c}$$

Where $M_b=\left(M^{tr}\right)M$ is the auxiliary connection matrix.

4.4 Full magnetic field – Electric circuits coupling model

Combining equation (25), (30) and (34) a system of coupled equations is obtained:

$$\begin{bmatrix}[S+M](A_{k+1}^{q+1})+S^{AGE} & \left[D^r\right]^{tr} & \left[D^s\right]^{tr}KK^{tr}\\ \left[D^r\right] & \left[C^r\right] & 0\\ K\left[D^s\right] & 0 & \left[G^s\right]\end{bmatrix}\times\begin{bmatrix}A^{q+1}\\ \left(U_m^r\right)^{q+1}\\ \left(I_{1,2}^s\right)^{q+1}\end{bmatrix}_{k+1}=$$

$$-\begin{bmatrix}[S-M]\left(A_k^q\right)+S^{AGE} & \left[D^r\right]^{tr} & \left[D^s\right]^{tr}KK^{tr}\\ \left[D^r\right] & \left[C^r\right] & 0\\ K\left[D^s\right] & 0 & \left[H^s\right]\end{bmatrix}\begin{bmatrix}A^q\\ \left(U_m^r\right)^q\\ \left(I_n^s\right)^q\end{bmatrix}\ -\ \begin{bmatrix}0\\ \left(\left[G^r\right]I_m^r\right)_k\\ \left[C^s\right]\left[\left(V_n^s\right)_{k+1}+\left(V_n^s\right)_k\right]\end{bmatrix} \tag{36}$$

Because of the non linearity of the core material, the stiffness matrix [S] depends on the nodal values of the magnetic vector potential. After applied the Newton Raphson iteration

method, a final algebraic system of equations for the nonlinear time-stepping simulation of the electrical machine is obtained such as:

$$\begin{bmatrix} P(A_{k+1}^{q}) & \left[D^{r}\right]^{tr} & \left[D^{s}\right]^{tr} KK^{tr} \\ \left[D^{r}\right] & \left[C^{r}\right] & 0 \\ K\left[D^{s}\right] & 0 & \left[G^{s}\right] \end{bmatrix} \begin{bmatrix} \Delta A_{k+1}^{q+1} \\ \Delta\left(U_{m}^{r}\right)_{k+1}^{q+1} \\ \Delta\left(J_{1,2}^{s}\right)_{k+1}^{q+1} \end{bmatrix} = \begin{bmatrix} \Re^{f}\left(A_{k+1}^{q}, \left(U_{m}^{r}\right)_{k+1}^{q}, \left(J_{1,2}^{s}\right)_{k+1}^{q}\right) \\ \Re^{r}\left(A_{k+1}^{q}, \left(U_{m}^{r}\right)_{k+1}^{q}\right) \\ \Re^{s}\left(A_{k+1}^{q}, \left(J_{1,2}^{s}\right)_{k+1}^{q}\right) \end{bmatrix} \tag{37}$$

Where P is the Jacobian matrix system expressed through the following matrices elements (Joao, et al., 2003; Arkkio, 1987; Benali, 1997):

$$S_{ij} = S^{AGE} + \iint_{\Omega} \nu(A_{k+1})(\nabla N_i)\left(\nabla N_j\right) d\Omega \tag{38.a}$$

$$P_{ij} = S^{AGE+} S_{ij} + J_{ij} = S^{AGE} + S_{ij} \quad + \iint_{\Omega} \sum_{j=1}^{N_n} \left(\frac{\partial \upsilon\left(A_j\right)_{k}^{q}}{\partial A_j} \right) \left(\nabla N_i\right) \cdot \left(\nabla N_j\right) d\Omega \tag{38.b}$$

$$M_{ij} = \iint_{\Omega} \frac{2\sigma}{\Delta t} N_i N_j \, d\Omega \tag{38.c}$$

5. Mechanical model and movement simulation

5.1 Movement simulation technique

For modelling the movement in rotating electrical machines using the Air-Gap-Element (AGE), the space discretised domain is commonly split up into two subdomains, a stator Ω_{stator}, and rotor Ω_{rotor} meshed domains, and the unmeshed air gap with Γ^{AGE} boundary (Fig. 5).

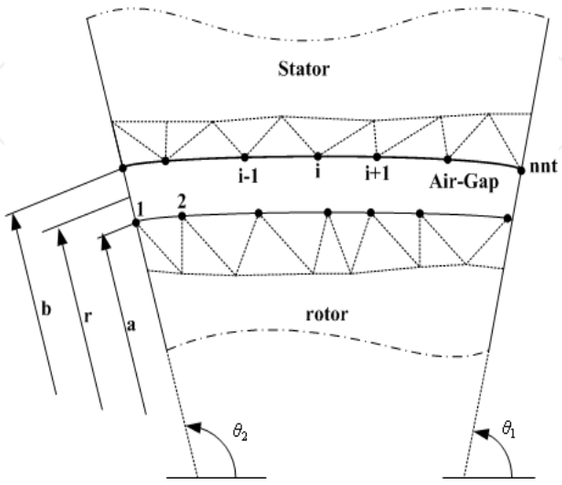

Fig. 5. Air-Gap Element (macro-element).

In a general step-by-step solution of the magnetic field in rotating electrical machines, the stator and rotor magnetic field equations are expressed in their own coordinate systems. The solutions of both fields equations are matched to each other in the air-gap. The rotor is rotated at each time step by an angle corresponding to the mechanical angular frequency, this means that a new finite element mesh in the air gap has to be constructed. The basic form of the air gap element matrix general terms is given by the expression:

$$A(a,b,r,\theta)=\sum_{j=1}^{nntl}A_i\left[\frac{1}{2}a_{0j}+\sum_{r=1}^{\infty}\left[a_{rj}\cos(\lambda_r\theta)+b_{rj}\sin(\lambda_r\theta)\right]\right]=\sum_{j=1}^{nnt}\left(N_j^{AGE}(a,b,r,\theta)\right)\cdot A_j^{\Gamma_{AGE}} \quad (39)$$

Where $\left(a_{0j},a_{rj},b_{rj},\lambda_r\right)$ are the Fourier's expansion coefficient which depends on the air-gap nodes coordinates locations, nnt is the total numbers of the air-gap nodes.

The movement simulation is take into account through the expression (39) while computing the associated matrix of the air-gap element given by the line integral term defined in the formulation (24). The air-gap-element matrix is given as follow:

$$\oint_{\Gamma^{AGE}}\upsilon_o\sum_{j=1}^{nnt}\left\{A_j^{AGE}\right\}\frac{\partial}{\partial n}\left(N_j^{AGE}(r,\theta)\right)d\Gamma^{AGE}=\left[S^{AGE}\right]\left\{A_j^{AGE}\right\} \quad (40)$$

For a complete development of the air gap element, the reader are invited to detailed implementation given in (Abdel-Razek, et al., 1982; Joao, et al., 2003).

5.2 Mechanical equations and torque computation

In a general case the magnetic field and electric circuits equations are coupled to the rotor mechanical equation through the electromagnetic torque. This includes the interaction between mechanical and electromagnetic quantities (Ho, et al., 2000). The mechanical differential system equations of speed and angular displacement is given as follow:

$$\frac{d}{dt}\begin{bmatrix}\omega\\ \theta\end{bmatrix}=\begin{bmatrix}-\frac{f}{J_m} & 0\\ 1 & 0\end{bmatrix}\begin{bmatrix}\omega\\ \theta\end{bmatrix}+\begin{bmatrix}\frac{1}{J_m}\left(C_{em}(t)-C_{load}\right)\\ 0\end{bmatrix} \quad (41)$$

At each step time, the computed electromagnetic torque is introduced in the mechanical model (41) solved using the fourth order Rung- Kutta method to get the rotor angular displacement and speed. The electromagnetic torque is computed from Maxwell's Tensor as a function of radial and tangential components of the magnetic flux density:

$$C_{em}=\frac{pr^2L_\delta}{\mu_0}\int_{\theta_1}^{\theta_2}B_rB_\theta d\theta \quad (42)$$

Where r is the rotor external radius, and p the number of poles pairs. The magnetic flux density components $\left(B_r,B_\theta\right)$ are computed in the air gap boundaries through the derivatives expression of the analytical magnetic vector potential shape functions (39).

6. Simulation results and discussions

6.1 Algorithm of Non-linear step by step finite element solver

The theory of the previous paragraphs is applied for the simulation of an induction motor in different operating modes. Two cases are studied, the first one concern the electric transient state simulation of induction motor while considering constant speed, and the second one treat the general electromagnetic-mechanical transient state simulation. The solution process of the electromagnetic-mechanical non-linear transient model is summurised by the following chart (see Fig.6).

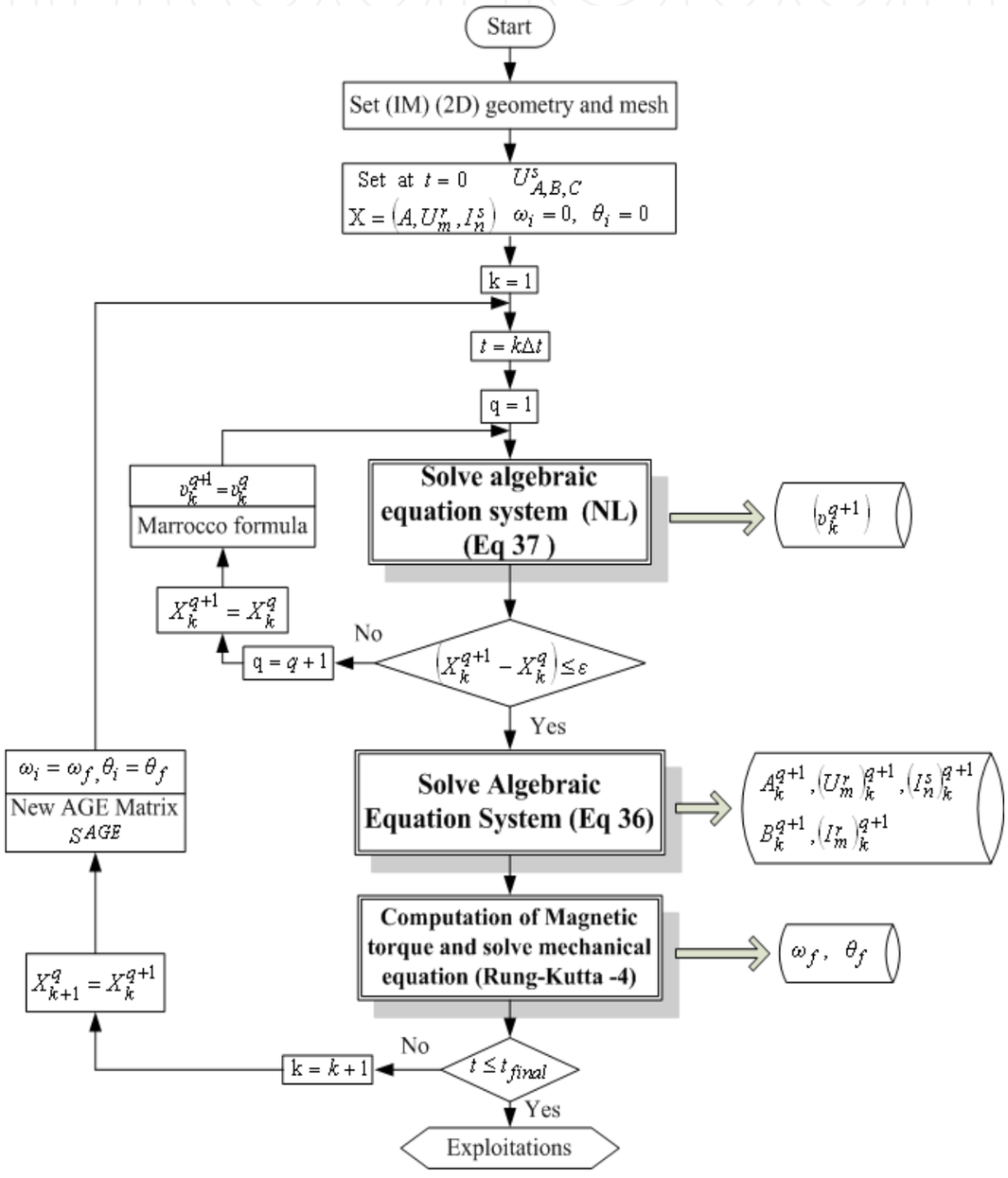

Fig. 6. General algorithm for induction machine numerical analysis.

6.2 Presentation of the studied induction motor

The considered simulated system to apply the model of the present works is an three phase induction motor Leroy Sommer (Mezani, 2004). The poles number is four, the rated power, the efficiency, and voltage are respectively 5.5KW, 84.26% and 380V. The stator windings and the rotor cage (bars-end rings) are made respectively with cooper and aluminium materials. More detailed characteristics of the motor are presented in Table. 1.

Geometrical components	Values (mm)	Physical components	Values
Stator core external diameter	168.0	Rated nominal current	11.62A
Stator core internal diameter	130.0	Nominal torque	37 N.m
Rotor core external diameter	109.2	Power factor	0.865
Rotor core inernal diameter	66.4	Moment of inertia	0.014 (Kg.m2)
Axial length	160.0	Friction coefficient	0.011 (1/ms)
Stator conductors per slot	19	Slip	4.13%
Number of stator slot	48 slots	Stator phase resistance	1.4Ω
Number of rotor slot	24 bars	Stator phase inductance	0.2 mH

Table 1. Studied induction motor geometrical and physical datas.

The stator and rotor slots geometrical dimensions are detailed in the following Fig. 7. To reduce the computational time due to nodes number of the finite element mesh and the geometrical complexity, usually the electrical machines models are created on the smallest symmetrical part of the machine. The (Fig. 8) shows the finite element mesh of the motor studied domain where only ¼ of the motors. The mesh containing 3204 nodes and 5623 first order triangular element is obtained using the Matlab PdeTool mesh automatic generator. We note that the air-gap between the stator and rotor meshes is not meshed and coupled together through the air-gap matrix (40). Homogeneous Dirichlet boundary condition is imposed for the external and internal motor radius, and anti-periodic ones at the other boundaries.

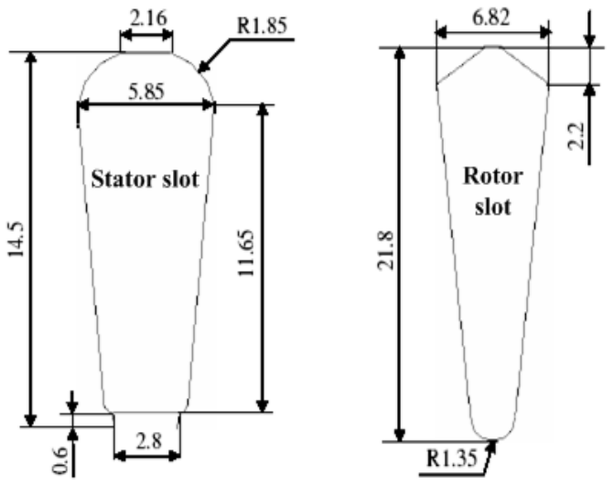

Fig. 7. Gometrical dimensions of the motor slots.

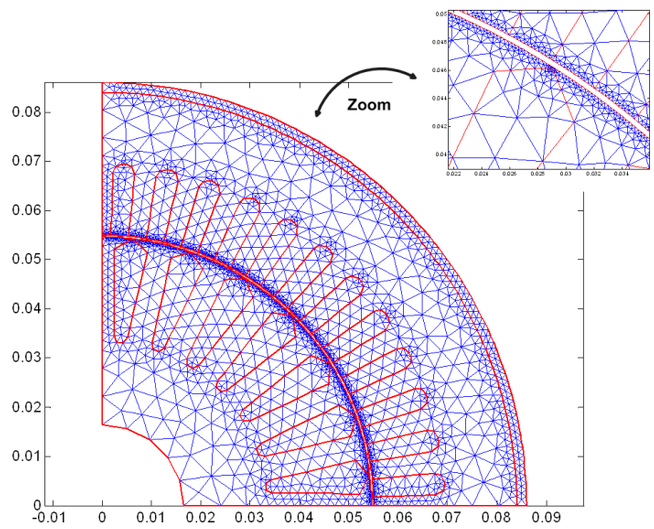

Fig. 8. Finite Element Mesh with (AGE).

6.3 Electromagnetic transient operating condition with constant speed

Results of this part concern the transient electromagnetic state simulation, at no load and nominal operation modes while the speed is considered constant. The electromagnetic transient is simulated while considering that the motor is operating in steady state with constant speed. Stator and rotor meshes are coupled by air-gap-element matrix. The constant speed value is equal to 1495 tr/mn and 1348 tr/mn respectively for the no-load and nominal modes. Since the mechanical phenomena is not considered, the speed is constant and the rotor displacement is not taken into account. The air-gap-element matrix is calculated only once. At each step time, the algebraic system (37) corresponded to Newton-Raphson algorithm is iteratively solved in order to get the magnetic permeability value. The latest is then used to establish the algebraic system (36) which the solution lead to the values of the magnetic vector potential, stator windings currents and the rotor bars voltages.

The stator windings currents wave forms corresponded to the electromagnetic transient state of the no-load and nominal conditions are respectively shown in Fig. 9 and Fig. 10. We note that, in agreement with the theory a high starting currents are obtained which decreases quickly because of the small electromagnetic durations. Electromagnetic torque for the no-load and nominal electromagnetic transient operations is given by the Fig. 11. After a brief transient duration the torque is stabilized at 4.5 N.m and 37.3 N.m values respectively for no load and nominal conditions.

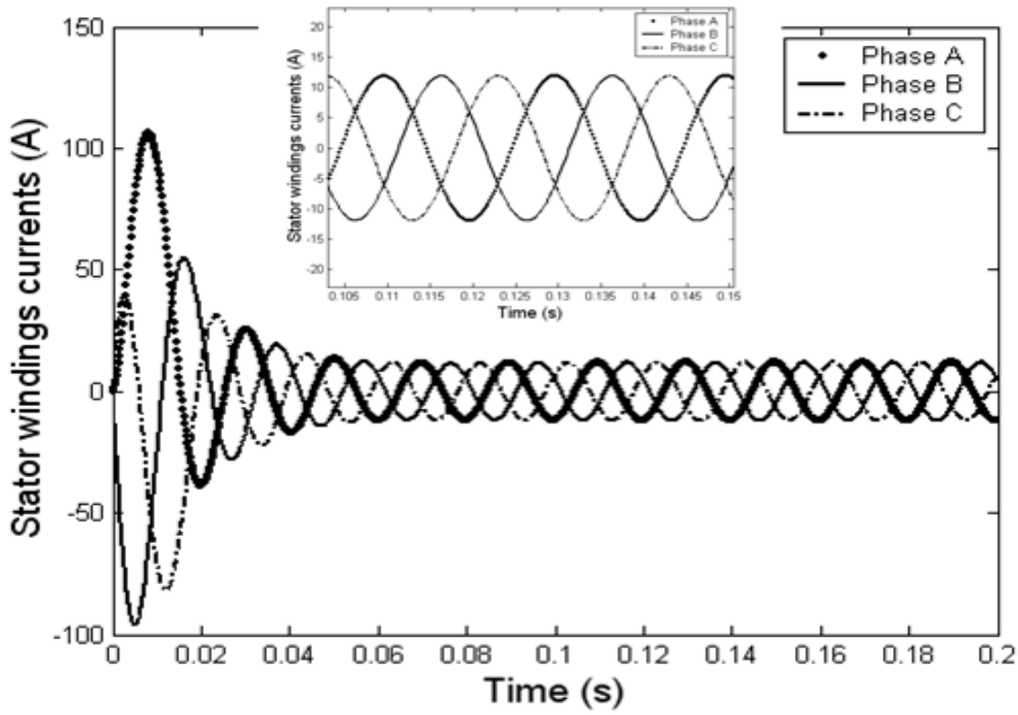

Fig. 9. Stator currents in no-load mode.

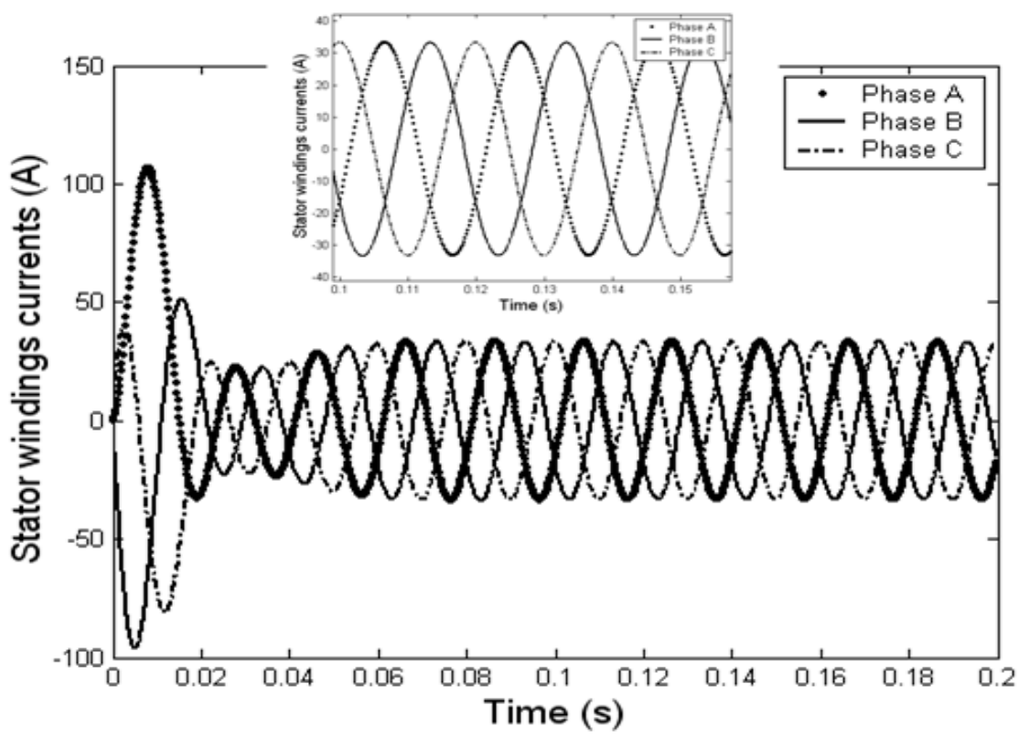

Fig. 10. Stator currents nominal mode.

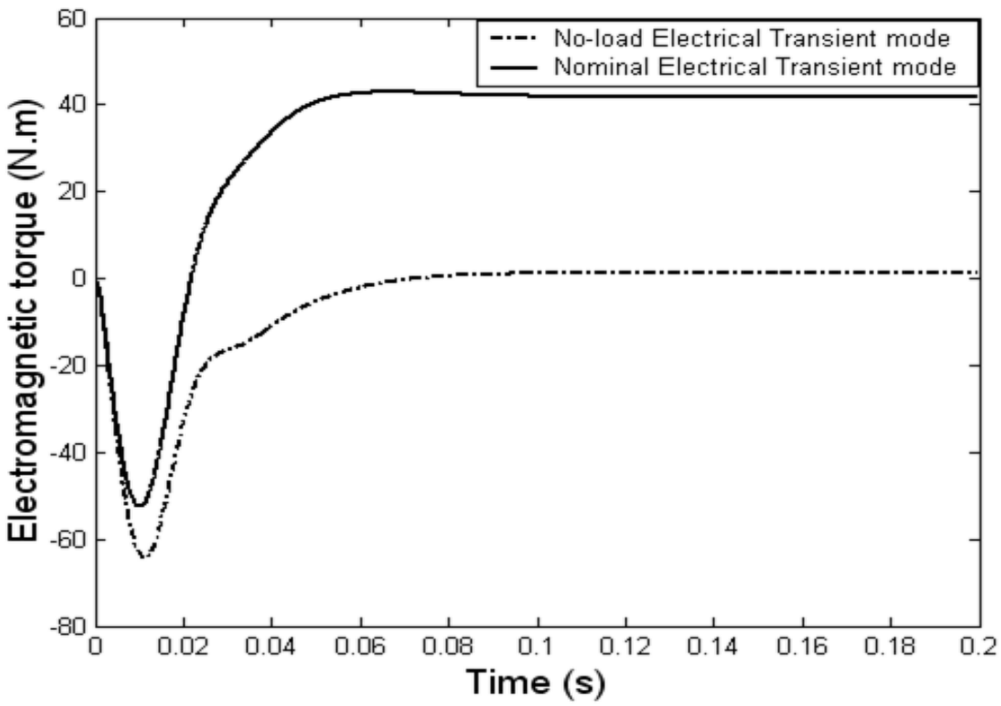

Fig. 11. Electromagnetic torque at no-load and nominal modes.

6.4 Electromagnetic-mechanical transient operating with direct start

Results of this part concern the transient electromagnetic-mechanical general simulation, at no load and load direct start operation modes. The solution process detailed by the Fig.6 is summarized by the following steps. Firstly, the algebraic equation system (37) is solved to get the magnetic reluctivity associated to the voltage level at each step time. Secondly, the algebraic equation system (36) is solved, which permit us to know the stator windings currents, the rotor bar voltages, and the magnetic vector potential which lead to deduce the magnetic flux density, and permit the computation of the electromagnetic torque. The latest is introduced in the mechanical model, which solution leads to the speed and angular displacement of the rotor. Since the mechanical phenomena is considered, the rotor displacement is taken into account, the air-gap-element matrix corresponded to each rotor position is calculated at each displacement step.

The motor simulations concerns a direct start loaded condition with load torque of 10 N.m. The stator windings currents wave forms are given by the Fig. 12 and Fig. 13. Motor angular speed, and electromagnetic torque are given by the Fig. 14, and Fig. 15, respectively.

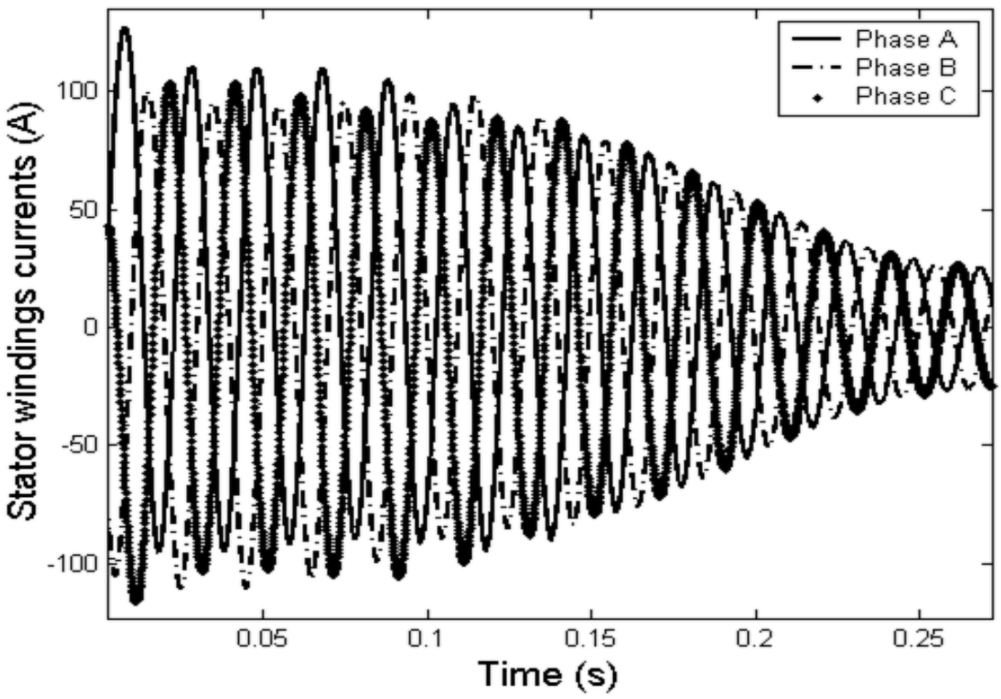

Fig. 12. Stator windings currents for direct start loaded motor.

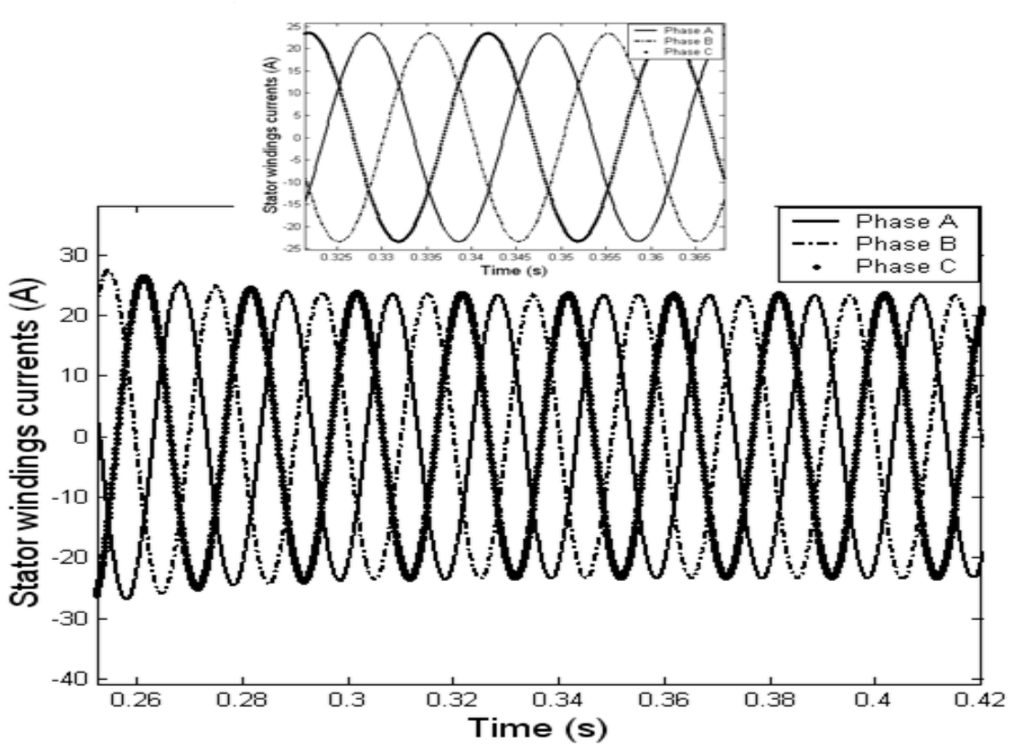

Fig. 13. Steady state stator windings currents for loaded direct start motor.

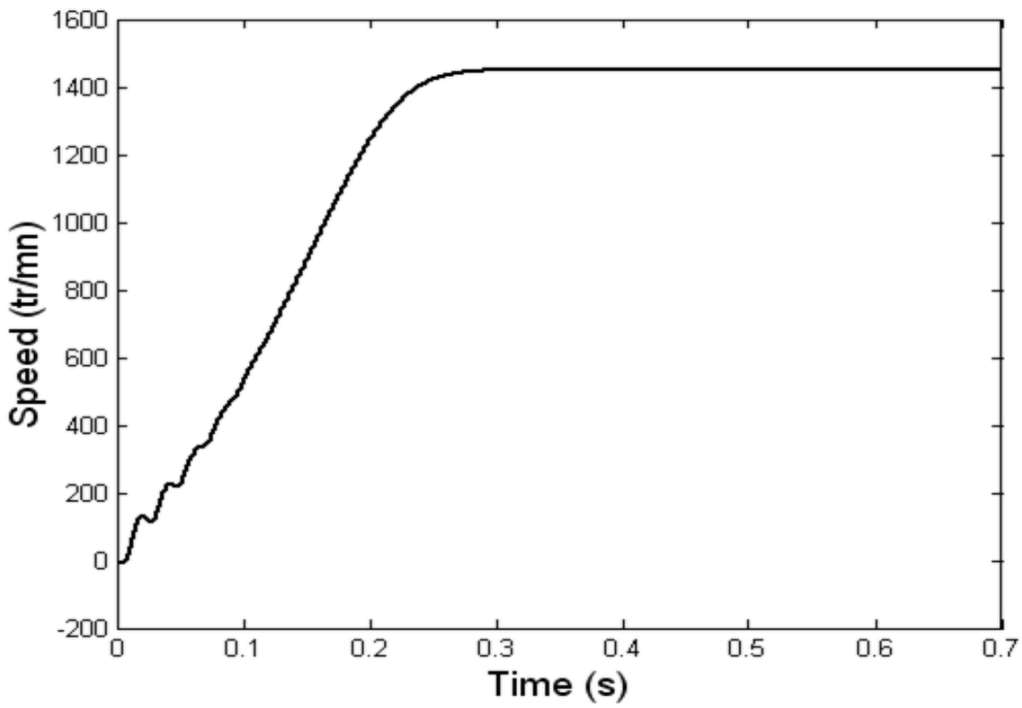

Fig. 14. Speed for loaded direct start motor.

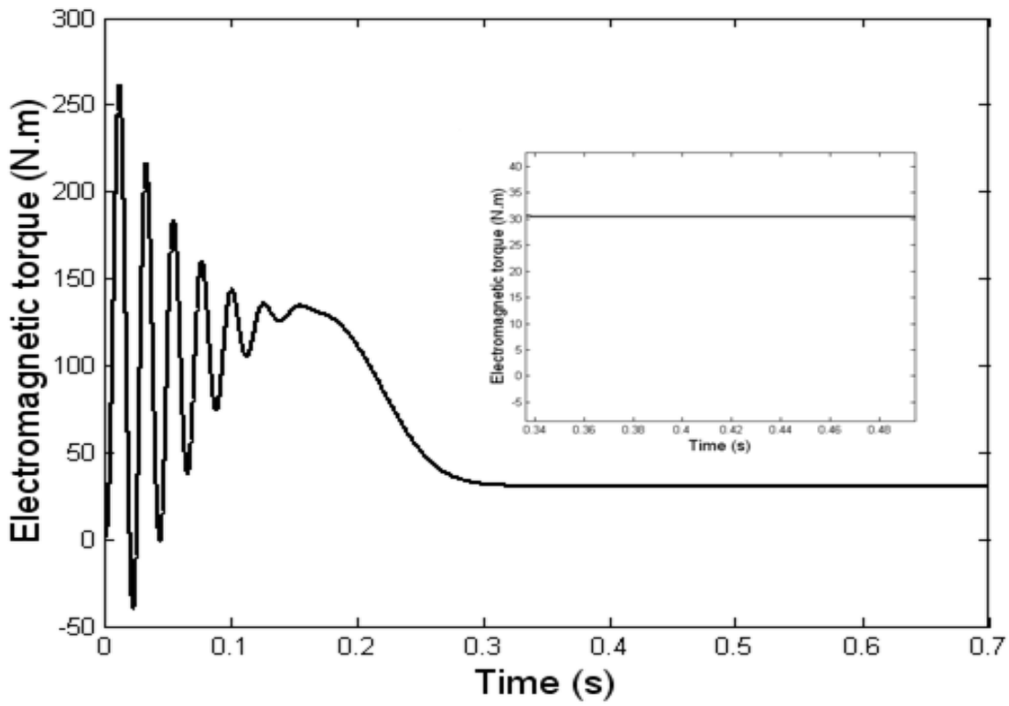

Fig. 15. Electromagnetic torque for loaded direct stat motor.

From the transient stator currents results given by the Fig. 12 we note a high starting currents which reach to nominal steady state values after average half periods such as given by the Fig. 13. The several ascillation of the currents transients behavior is due to the strong electromagnetic and mechanical interaction through theirs corresponded time constants.For the rotor speed given by the Fig.14, we note that after some modulations at the motor start, gthe speed increase linearely till it steady state values according to mechanical first order differential equation. The Fig. 15 of electromagnetic torque show that after some periods oft he magnetic duration the torque reach to it steady state value of average 37.3 N.m.

7. Conclusion

This chapter goal is to present a detailed finite element method use to solved partial differential equation of electromagnetic phenomena occurred in induction motor. The magnetic field equation expressed in term of magnetic vector potential strongly coupled with the electric circuits equations of the stator windings and rotor cage are solved using the nodal based finite element process. The resulting nonlinear time-dependent algebraic differential equations system obtained from the finite element formulation is solved using step-by-step numerical integration based on the Crank-Nicholson scheme, combined to the Newton-Raphson iterative process for handling the magnetic material non-linearity. The electromagnetic and mechanic interaction is considered firstly by the computation of the electromagnetic torque by the Maxwell stress tensor responsible of the rotor displacement, and secondly by solving the mechanical motional equation to get the new rotor angular position. Since the motor is meshed only once, the rotor movement is taking into account by the macro-element method which lead to an air-gap matrix of the movement. The validation of the model is performed through simulation of an induction motor in no-load and loaded direct start operating modes. The numerical results are in good agreement with corresponding results appearing in the recent literature. The contribution of this work can be applied to analyze a large class of electrical machines, and offers an important support for students, teachers and industrial employers for understanding the basis of numerical modelling of electrical machines.

8. References

Abdel-Razek, A.; Coulomb, J.L.; Féliachi, M. & Sabonnadière, J.C. (1982), Conception of an Air-Gap Element for the Dynamic Analysis of the Electromagnetic Field in Electric Machines, *IEEE Transaction On Magnetics,* Vol.18, No.2, (March 1982), pp. 655-659, ISSN 0018-9464.

Arkkio, A. (1987), Analysis of induction motors based on the numerical solution of the magnetic field and circuit equations. PhD Dissertation, Helsinki University of Technology, Sweeden.

Benali, B. (1997), Contribution à la modélisation des systèmes électrotechniques à l'aide des formulations en potentiel : Application à la machine asynchrone, Doctorat thesis, University of Sciences and Technology of Lille, France.

Binns, K.J.; Lawrenson, P.J, & Trowbridge, C.W. (1994), The Analytical and Numerical Solution of Electrical and Magnetic Fields, In: Wiley, (Ed.), ISBN 0471924601, Chichester, England.

Brauer, J.R. ; Ruehl, J.J, & Hirtenfelder, F. (1985), Coupled nonlinear electromagnetic and structural finite element analysis of an actuator excited by an electric circuit. *IEEE Transaction On Magnetics,* Vol.31, No.3, (May 1985), pp. 1861-1864, ISSN 0018-9464.

Dreher, T.; Perrin-Bit, R.; Meunier, G. & Coulomb, J.L. (1996), A 3D finite element modelling of rotating machines involving movement and external circuit, *IEEE Transactions on Magnetics,* Vol.32, No.4, (April 1996), pp. 1070-1073, ISSN 0018-9464.

Hecht, F.; Marrocco, A.; Piriou, F. & Abdel-Razek,A. (1990), Modélisation des systèmes électrotechniques par couplage des équations électriques et magnétiques, *Revue de Phyique Applique,*Vol.25, (July 1990), pp. 649-659, ISSN 0018-9464.

Ho, S.L.; Li, H.L.; Fu, W.N. & Wong, H.C. (2000), A novel approach to circuit-field-torque coupled time stepping finite element modelling of electrical machines. *IEEE Transactions on Magnetics,* Vol.36, No. 4, (July 2000), pp. 1886-1889, ISSN 0018-9464.

Ho, S.L., & Fu, W.N. (1997), A comprehensive approach to the solution of direct-coupled multi-slice model of skewed motors using time stepping eddy-current FEM. *IEEE Transactions on Magnetics,*Vol.33, No.3, (May 1997), pp. 2265-2273, ISSN 0018-9464.

Joao, P.; Bastos, A. & Sadowski, N. (2003), Electromagnetic Modeling by Finite Element Methods, Marcel Dekker Inc, (Ed.), ISBN 0824742699, New York, United States.

Kanerva, S. (2005), Simulation of electrical machines, circuits and control systems using finite element method and system simulation, PhD. Dissertation, Helsinki University of Technology, Sweden.

Mezani, S. (2004), Modélisation électromagnétique et thermique des moteurs à inductions en tenant compte des harmoniques d'espaces, Doctorat thesis, Polytechnical institut of Loraine, Nancy, France.

Neagoe, C. & Ossart, F. (1994), Analysis of convergence in non linear magnetostatics finite element problems. *IEEE Transactions on Magnetics,* Vol.30, No.5, (September 1994), pp. 2865-2868, ISSN 0018-9464.

Nougier, J.P. (1999), Methodes de Calcul Numeriques, In: Masson, (Ed.), Oxford University press, ISBN 0-19-511767-0, New York, United state.

Piriou, F. & Abdel-Razek, A. (1990), A model for coupled magnetic-electric circuits in electric machines with skewed slots. *IEEE Transactions on Magnetics*, Vol.26, No.2, (March 1990), pp. 1096-1100, ISSN 0018-9464.

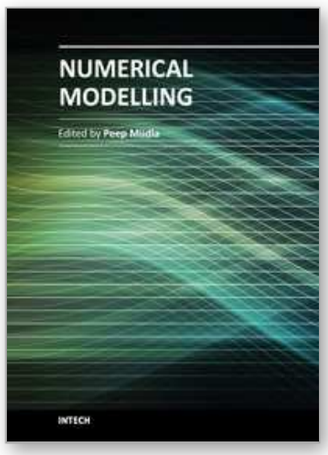

Numerical Modelling

Edited by Dr. Peep Miidla

ISBN 978-953-51-0219-9
Hard cover, 398 pages
Publisher InTech
Published online 23, March, 2012
Published in print edition March, 2012

This book demonstrates applications and case studies performed by experts for professionals and students in the field of technology, engineering, materials, decision making management and other industries in which mathematical modelling plays a role. Each chapter discusses an example and these are ranging from well-known standards to novelty applications. Models are developed and analysed in details, authors carefully consider the procedure for constructing a mathematical replacement of phenomenon under consideration. For most of the cases this leads to the partial differential equations, for the solution of which numerical methods are necessary to use. The term Model is mainly understood as an ensemble of equations which describe the variables and interrelations of a physical system or process. Developments in computer technology and related software have provided numerous tools of increasing power for specialists in mathematical modelling. One finds a variety of these used to obtain the numerical results of the book.

InTech Europe
University Campus STeP Ri
Slavka Krautzeka 83/A
51000 Rijeka, Croatia
Phone: +385 (51) 770 447
Fax: +385 (51) 686 166
www.intechopen.com

InTech China
Unit 405, Office Block, Hotel Equatorial Shanghai
No.65, Yan An Road (West), Shanghai, 200040, China
中国上海市延安西路65号上海国际贵都大饭店办公楼405单元
Phone: +86-21-62489820
Fax: +86-21-62489821

IntechOpen